AGU PUBLICATIONS

JGR

Journal of Geophysical Research: Solid Earth

RESEARCH ARTICLE
10.1002/2015JB011900

Key Points:
- Interlayer bonding energy (ILBE) is estimated by DFT calculations
- The relationship between ILBE and the friction coefficient is less clear
- Frictional strength should be discussed on the basis of the ILBE

Supporting Information:
- Tables S1–S3

Correspondence to:
H. Sakuma,
SAKUMA.Hiroshi@nims.go.jp

Citation:
Sakuma, H., and S. Suehara (2015), Interlayer bonding energy of layered minerals: Implication for the relationship with friction coefficient, *J. Geophys. Res. Solid Earth*, *120*, 2212–2219, doi:10.1002/2015JB011900.

Received 21 JAN 2015
Accepted 11 MAR 2015
Accepted article online 16 MAR 2015
Published online 15 APR 2015

Interlayer bonding energy of layered minerals: Implication for the relationship with friction coefficient

Hiroshi Sakuma[1] and Shigeru Suehara[2]

[1]Environmental Remediation Materials Unit, National Institute for Materials Science, Tsukuba, Japan, [2]Computational Materials Science Unit, National Institute for Materials Science, Tsukuba, Japan

Abstract The frictional strength of layered minerals is an important component of fault slip physics. A low-friction coefficient of these minerals has been attributed to the interlayer bonding energy (ILBE) of their weak interlayer bonding. The ILBE used for discussing the friction coefficient is based on a simple electrostatic calculation; however, the values should be revisited by precise calculations based on quantum mechanics. In this study, the ILBEs of layered minerals were calculated by using the density functional theory (DFT) method with van der Waals correction. The ILBEs calculated by the simple electrostatic method for hydrogen-bonding minerals such as kaolinite, lizardite, gibbsite, and brucite strongly overestimated the reliable energies calculated by the DFT method. This result should be ascribed to the inaccurate approximation of the point charges at the basal plane. A linear relationship between the experimentally measured friction coefficients of layered minerals and the ILBEs determined by the simple method was not confirmed by using the reliable ILBEs calculated by our DFT method. The results, however, do not remove the possibility of a relationship between interlayer bonding energy and the friction coefficient because the latter, used for comparing the former, was obtained through experiments conducted under various conditions.

1. Introduction

The presence of sheet structure minerals such as micas and clays, which are abundant in natural faults, reduces the maximum friction coefficient of faults to 0.2–0.8 [*Behnsen and Faulkner*, 2012, 2013; *Boutareaud et al.*, 2012; *Byerlee*, 1978; *Carpenter et al.*, 2011; *Ikari et al.*, 2009; *Lockner et al.*, 2011; *Logan and Rauenzahn*, 1987; *Moore and Lockner*, 2004, 2007; *Oohashi et al.*, 2013; *Shimamoto and Logan*, 1981; *Wintsch et al.*, 1995]. However, the friction coefficients of common rocks are nearly constant at 0.6–1.0 [*Byerlee*, 1978]. The fundamental physics laws resulting in the low-friction coefficients of sheet structure minerals are important for understanding fault slip and earthquake occurrence. These low coefficients of friction have been explained from the perspective of interlayer bonding energy (ILBE) connecting the basal planes of these sheet structure minerals [*Moore and Lockner*, 2004; *Morrow et al.*, 2000]. A simple linear relationship between the friction coefficient and ILBE has been reported [*Moore and Lockner*, 2004], which appears to represent the hypothesis that major slip planes lie parallel to the basal planes. However, the linear dependence of friction on ILBE as discussed by Moore and Lockner was not observed in similar shear experiments for layered minerals [*Behnsen and Faulkner*, 2012]. Although different particle sizes and shapes of minerals investigated by these measurements may influence friction [*Abe and Mair*, 2009; *Anthony and Marone*, 2005; *Frye and Marone*, 2002; *Henderson et al.*, 2010; *Mair et al.*, 2002; *Morgan*, 1999], we should consider the accuracy of the ILBE, or separation energy, determined by simple electrostatic calculations [*Giese*, 1974, 1978] before discussing particle size distribution and shape.

The ILBE used for the discussion was based on a theoretically derived interlayer bonding energy [*Giese*, 1974, 1978]. Several approximations in this method include the empirical potential function, fixed atomic position, fixed formal charge of ions, and finite separation distances between two layers. Through recent developments in computational physics and chemistry, however, the ILBE can be calculated without using such approximations [*Sakuma*, 2013].

Herein, the ILBEs of sheet structure minerals were calculated by using the first-principles density functional theory (DFT) method as previously applied to muscovite [*Sakuma*, 2013]. DFT is rooted in quantum mechanics and has become a primary tool for calculating the electronic structures of minerals. With this

Table 1. Sheet Structure Minerals Tested in this Study

Mineral	Formula Unit	Estimated Major Interaction Between Layers	Structure Type
Pyrophyllite	$Al_2(OH)_2[Si_4O_{10}]$	vdW[a]	Dioctahedral[b]
Talc	$Mg_3(OH)_2[Si_4O_{10}]$	vdW	Trioctahedral[c]
Kaolinite	$Al_2(OH)_4[Si_2O_5]$	Hydrogen bond, vdW	Dioctahedral
Lizardite	$Mg_3(OH)_4[Si_2O_5]$	Hydrogen bond, vdW	Trioctahedral
Gibbsite	$Al(OH)_3$	Hydrogen bond, vdW	Dioctahedral
Brucite	$Mg(OH)_2$	Hydrogen bond, vdW	Trioctahedral
Muscovite	$KAl_2(OH)_2[Si_3AlO_{10}]$	Coulomb, vdW	Dioctahedral
Phlogopite	$KMg_3(OH)_2[Si_3AlO_{10}]$	Coulomb, vdW	Trioctahedral

[a]Van der Waals interaction.
[b]Two thirds of the octahedral sites are filled with trivalent Al^{3+}; the remaining third is vacant.
[c]All octahedral cation sites are occupied with divalent Mg^{2+}.

method, the calculated ionic configurations, lattice constants, and elasticity of ionic and covalently bound minerals are accurate. Moreover, the error of the lattice constants is within a few percentage points of the experiment [*Milman et al*., 2000]. The high reproducibility of lattice constants and elasticity guarantees precise prediction of the ILBEs of sheet structure minerals without using the empirical approximation of charge distributions in the minerals such as fixed formal and partial point charges. However, one limitation of the DFT method is the description of van der Waals force [*Johnson et al*., 2009; *Björkman et al*., 2012]; the intermolecular binding energies among small molecules calculated by the DFT method underestimate the energy obtained from precise experiments. This limitation is ascribed to the inability of electronic exchange-correlation functionals to describe the force [*Koch and Holthausen*, 2001]. Methods for developing a new exchange-correlation functional [*Kummel and Kronik*, 2008; *Langreth et al*., 2005; *Dion et al*., 2004] and empirical correction by using an analytical function [*Grimme*, 2006; *Grimme et al*., 2010] have been proposed to avoid such a problem [*Björkman et al*., 2012]. In the present study, we employ mainly the empirical van der Waals correction (DFT-D2) [*Grimme*, 2006]. ILBEs calculated by using the DFT method are compared with the friction coefficients of gouge minerals. The friction coefficients of the layered gouge minerals are discussed from the perspective of ILBE and particle shape.

2. Minerals and Methods

We calculated the ILBEs of the sheet structure minerals listed in Table 1. The sheet structure minerals tested in this study were categorized into two types according to the cations in the octahedral sites. Two thirds of the octahedral sites in pyrophyllite, kaolinite, gibbsite, and muscovite are occupied by trivalent Al^{3+}; the remaining third is vacant. Such minerals are categorized as dioctahedral minerals. All octahedral sites in talc, lizardite, brucite, and phlogopite are occupied by divalent Mg^{2+}; these minerals are trioctahedral. Pyrophyllite, talc, muscovite, and phlogopite are 2:1-type layer silicates and consist of an $[MO_6]$ octahedral sheet (M = Al or Mg) sandwiched between two $[TO_4]$ tetrahedral sheets (T = Si or Al). Gibbsite and brucite have a layer of Al^{3+} or Mg^{2+} sandwiched between two sheets of hexagonally packed hydroxyl ions. These Al^{3+} and Mg^{2+} occupy the octahedral site. The major forces connecting the sheets are hydrogen bonding and van der Waals force. Pyrophyllite and talc have no structural layer charges; therefore, a major component of the separation between their basal planes is van der Waals force. Muscovite and phlogopite have negative structural layer charges (−1/formula unit), and the basal planes are connected by the presence of interlayer cations of K^+. Therefore, the major separation force of muscovite and phlogopite appears to be electrostatic Coulomb force. Kaolinite and lizardite are 1:1-type layer silicates and consist of one octahedral sheet and one tetrahedral sheet. All tetrahedrals in the sheet are oriented in one direction, and a gibbsite or brucite layer is joined to the sheet. A major component of the separation force is the hydrogen-bonding force between hydroxyl groups on octahedral sites and oxygen atoms of SiO_4 tetrahedra, as is van der Waals force among the atoms.

2.1. First-Principles Electronic State Calculations of Bulk Minerals

The lattice constants and structures for layered minerals were calculated by using the DFT method. The exchange and correlation functional has been described under the generalized gradient approximation of

Table 2. Calculated Lattice Constants of Sheet Structure Minerals[a]

Mineral (Cutoff Energy of Plane Waves) (*K* Points Mesh)	Lattice Constants	Calculated Lattice Constants by DFT-D2	Calculated Lattice Constants by PBE	Experiments (Reference)
Pyrophyllite (65 Ry) (4 × 2 × 2)	*a*	5.180 (+0.4%)	5.225 (+1.3%)	5.160
	b	8.999 (+0.4%)	9.075 (+1.2%)	8.966
	c	9.343 (−0.0%)	9.984 (+6.8%)	9.347
	α	90.96 (−0.2%)	90.85 (−0.4%)	91.180
	β	100.58 (+0.1%)	100.09 (−0.4%)	100.460
	γ	89.81 (+0.2%)	89.71 (+0.1%)	86.640
				[*Lee and Guggenheim*, 1981]
Talc (65 Ry) (4 × 2 × 2)	*a*	5.275 (−0.3%)	5.338 (+0.9%)	5.290
	b	9.148 (−0.3%)	9.248 (+0.8%)	9.173
	c	9.423 (−0.4%)	10.096 (+6.7%)	9.460
	α	90.88 (+0.5%)	90.34 (−0.1%)	90.460
	β	100.19 (+1.5%)	98.511 (−0.2%)	98.680
	γ	90.12 (+0.0%)	90.01 (−0.1%)	90.090
				[*Perdikatsis and Burzlaff*, 1981]
Kaolinite (65 Ry) (4 × 2 × 3)	*a*	5.185 (+0.6%)	5.222 (+1.3%)	5.1535
	b	8.999 (+0.6%)	9.066 (+1.4%)	8.9419
	c	7.328 (−0.9%)	7.476 (+1.2%)	7.3906
	α	91.86 (−0.1%)	91.52 (−0.4%)	91.926
	β	105.16 (+0.1%)	104.70 (−0.3%)	105.046
	γ	89.81 (+0.0%)	89.77 (−0.0%)	89.797
				[*Bish*, 1993]
Lizardite (60 Ry) (4 × 4 × 4)	*a*	5.301 (−0.5%)	5.380 (+1.0%)	5.3267
	c	7.223 (−0.4%)	7.418 (+2.3%)	7.2539
				[*Gregorkiewitz et al.*, 1996]
Gibbsite (60 Ry) (2 × 4 × 2)	*a*	8.676 (−0.1%)	8.789 (+1.2%)	8.684
	b	5.039 (−0.8%)	5.104 (+0.5%)	5.078
	c	9.484 (−2.6%)	9.683 (−0.5%)	9.736
	α	90.01 (0.0%)	89.99 (0.0%)	90.0
	β	93.52 (−1.1%)	92.10 (−2.6%)	94.54
	γ	90.00 (0.0%)	90.01 (0.0%)	90.0
				[*Saalfeld and Wedde*, 1974]
Brucite (60 Ry) (4 × 4 × 3)	*a*	3.121 (−0.7%)	3.169 (+0.8%)	3.142
	c	4.628 (−2.9%)	4.800 (+0.7%)	4.766
				[*Zigan and Rothbauer*, 1967]
Muscovite (60 Ry) (4 × 2 × 1)	*a*	5.199 (0.0%)	5.274 (+1.5%)	5.1988
	b	9.028 (0.0%)	9.158 (+1.5%)	9.0266
	c	19.827 (−1.4%)	20.544 (+2.2%)	20.1058
	β	95.53 (−0.3%)	95.37 (−0.4%)	95.78
				[*Richardson and Richardson*, 1982]
Phlogopite (65 Ry) (4 × 2 × 2)	*a*	5.268 (−0.9%)	5.349 (+0.6%)	5.3158
	b	9.148 (−0.6%)	9.282 (+0.9%)	9.2036
	c	10.146 (−1.6%)	10.762 (+4.4%)	10.3100
	α	89.96 (−0.0%)	90.35 (+0.4%)	90.0000
	β	100.11 (+0.2%)	103.13 (+3.2%)	99.8908
	γ	90.10 (+0.1%)	89.92 (−0.1%)	90.0000
				[*Redhammer and Roth*, 2002]

[a]The units of length are in Å; those of angles are in degrees.

Perdew-Burke-Ernzerhof (PBE) [*Perdew et al.*, 1996]. Pseudopotential methods [*Rappe et al.*, 1990; *Troullier and Martins*, 1991; *Vanderbilt*, 1990] were employed in this study because the valence electrons of most atoms should have a significant effect on the structure. The effect of core electrons was considered for K and Mg by using a nonlinear core correction method [*Louie et al.*, 1982]. The plane wave basis set was used for describing the electronic wave functions under the cutoff energies of 60–65 Ry for wave functions and 480–520 Ry for electron density. *K* point sampling was performed by using the Monkhorst-Pack method [*Monkhorst and Pack*, 1976], and the number of *k* point meshes listed in Table 2 was determined by confirming the total energy convergence. Semiempirical dispersion force corrections [*Barone et al.*, 2009; *Grimme*, 2006] for the PBE functional (DFT-D2) used in the calculations considered the van der Waals force responsible for reproducing the lattice constants of talc and pyrophyllite. The results calculated by other methods including

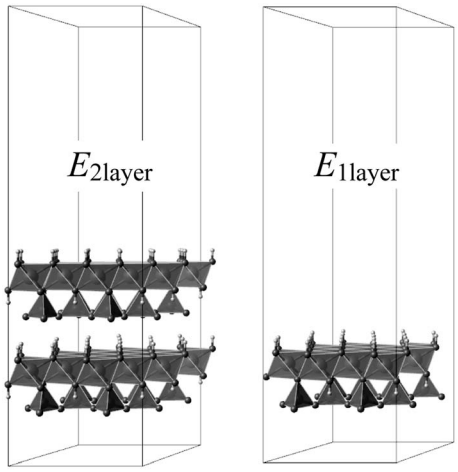

Figure 1. Schematic diagram explaining the manner in which calculated interlayer bonding energies (ILBEs) E_{ILBE} are determined for sheet structure minerals. E_{2layer} and E_{1layer} indicate two sheets and one sheet, respectively, in the total energy of the supercell. Boxes indicate the shapes of the supercells.

van der Waals interactions DFT-D3 [*Grimme et al*., 2010] and vdW-DF [*Klimeš et al*., 2011] did not change the conclusions of this study, as explained in the following section. The calculated lattice constants are listed in Table 2; all were determined by using the DFT-D2 method and were reliable within an underestimation of −2.9% relative to the experimental values. This result indicates that the interaction between basal planes is reasonable for all minerals examined. However, the lattice constants calculated by using the PBE method without van der Waals correction showed significant overestimation for the interlayer distances, particularly for pyrophyllite and talc, indicating the importance of van der Waals interaction for these minerals. These lattice constants calculated by using DFT-D2 and PBE for pyrophyllite, talc, kaolinite, and lizardite were consistent with results cited in previous research [*Tunega et al*., 2012].

2.2. First-Principles Electronic State Calculations of Interlayer Bonding Energy

The calculated ILBEs, E_{ILBE}, of sheet minerals were calculated by determining the energy difference between two layers versus one layer placed in a supercell, as shown in Figure 1. This procedure is the same as that shown in our previous study [*Sakuma*, 2013]. The cleavage plane was placed normal to the *c* axis. The *a* and *b* lengths and γ angle, determined by using the calculated lattice constants of the bulk minerals, are tabulated in Table S1 in the supporting information. A vacuum sufficient for removing the effect of periodic boundary conditions (>20 Å) was imposed on these layers. The *c* lengths were 45.9, 46.4, 36.1, 36.3, 37.9, 36.2, 40.1, and 50.7 Å for pyrophyllite, talc, kaolinite, lizardite, gibbsite, brucite, muscovite, and phlogopite, respectively. The numbers of *k* points are listed in Table S1. The artificial dipole generated by the asymmetry of the minerals in the periodic boundary condition was corrected by using a standard procedure [*Bengtsson*, 1999]. Interlayer cations were present in muscovite and phlogopite; half of the cations were separated to occur on one side of the surface. The initial position of the cations was the center of the ditrigonal rings composed by (Si_4Al_2) because on a muscovite surface, K^+ is more stable on the (Si_4Al_2) ring than on the (Si_5Al_1) ring [*Odelius et al*., 1997]. The criteria of total energy (<0.1 mRy) and force convergence (<1.0 mRy/bohr) were applied to calculate the total energy of the slab geometry. Although ionic optimization is essential for considering the effect of surface relaxation, this factor was not considered in the simple electrostatic calculations reported by *Giese* [1974, 1978]. To confirm the choice of van der Waals interaction in the DFT scheme, we compared the calculated ILBEs based on the different van der Waals methods of DFT-D2 [*Barone et al*., 2009; *Grimme*, 2006], DFT-D3 [*Grimme et al*., 2010], and vdW-DF (optB86b-vdW) [*Klimeš et al*., 2011], as plotted in Figure 2. The results determined by using the PBE method are shown in the figure for comparison. In these calculations, the size of the supercell was fixed at the same values as those of DFT-D2 listed in Table S2. The difference among the van der Waals corrections was insignificant for all minerals. The slight difference between the DFT-D2 methods calculated by the Quantum Espresso and Vienna ab initio simulation package (VASP) is attributed to differences in pseudopotentials; those used in VASP

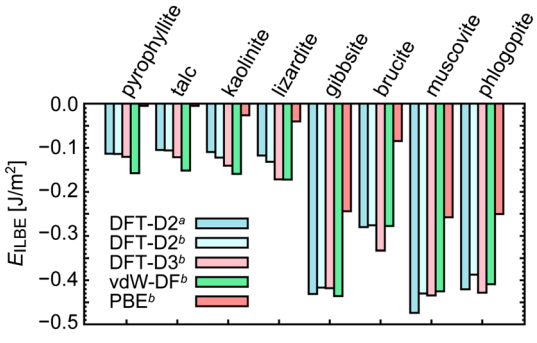

Figure 2. Calculated interlayer bonding energies (ILBEs) of layered minerals determined by using different schemes of van der Waals interaction. The size of the supercell was fixed to be the same as that determined on the basis of bulk minerals calculated by using DFT-D2[a]. The ILBEs were calculated by using Quantum Espresso[a] and VASP[b].

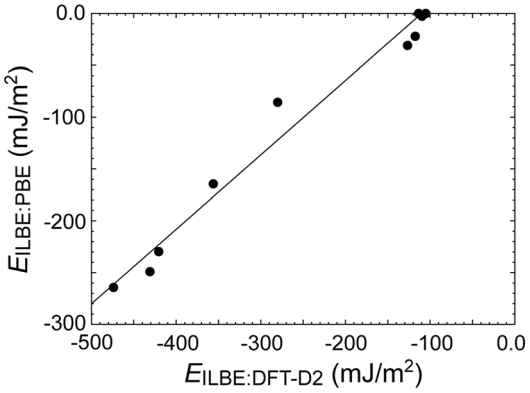

Figure 3. Interlayer bonding energies (ILBEs) calculated by DFT-D2 versus Perdew-Burke-Ernzerhof (PBE) functionals. The solid line is a fitted linear line expressed as $E_{ILBE:PBE} = 0.7179\ E_{ILBE:DFT-D2} + 78.952$.

are based on the projector augmented-wave method [*Kresse and Joubert*, 1999]. One of the most important points in these results is that the magnitude relationship of the ILBEs among these minerals was independent in the employed van der Waals methods. Hereafter, the DFT-D2 method is used for further discussion.

3. Results and Discussion

The calculated E_{ILBE} values are plotted in Figure 3. The E_{ILBE} without van der Waals correction or the PBE method for talc and pyrophyllite were not calculated and were set to zero because the optimized lattice constant perpendicular to the basal plane overestimated the experimental values by +6.7% for talc and +6.8% for pyrophyllite. The order of the ILBEs for these minerals was the same between the DFT-D2 and PBE calculations; therefore, the relationship can be described by a linear equation as shown in Figure 3. This indicates that the relative ILBE difference among minerals is independent of the incorporation of van der Waals correction. The experimentally determined E_{ILBE} value was available only for muscovite (-150 to -200 mJ/m^2) [*Christenson*, 1993]; this value is weaker than the calculated values obtained by using the DFT-D2 method (-481 mJ/m^2). This result can be attributed to a combination of factors from both experiments and calculations, as discussed in previous research [*Sakuma*, 2013]. These factors include the adsorption of contaminants on the mica surface, mismatched crystal axes among mica sheets, and the strong interaction in the underestimated interlayer distance (-2%) reflected by the DFT-D2 calculations. The calculated E_{ILBE} for all minerals studied herein corresponds to the lowest values based on ideal separation conditions.

A comparison of the ILBEs calculated by the Giese and DFT-D2 methods is shown in Figure 4. The ILBE obtained by the Giese method may be per unit area of *two surfaces*. This indicates that the energy calculated by Giese would be half of the quoted energy, if defined by the per unit area of *one surface*. In this paper, the energy per unit area of *one surface* is used as the ILBE calculated by Giese method. The ILBEs of 2:1-type minerals such as pyrophyllite, talc, muscovite, and phlogopite were consistent between the DFT-D2 and Giese methods. A significant overestimation by the Giese method was confirmed for 1:1-type clays such as kaolinite and lizardite and layered hydroxides such as gibbsite and brucite. The main attractive interaction between the layers in these minerals is hydrogen bonding. In the Giese method, the ILBEs are obtained by a simple electrostatic energy calculation based on the empirical charges of ions fixed to the formal charges such as +1 for a hydrogen atom. This assumption is inaccurate for describing hydrogen and covalent bonds in minerals because these bonds can be formed by sharing electrons among atoms. This formal charge assumption may be a primary reason for the overestimation of ILBEs for 1:1-type clays and layered hydroxides when using the Giese method. These comparisons indicate that the ILBE calculated by the DFT-D2 method should be used for discussing the frictional properties of layered minerals.

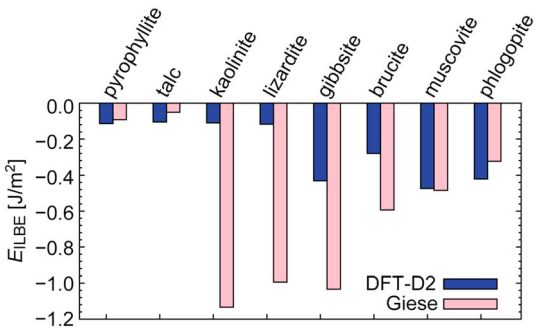

Figure 4. Comparison of the calculated interlayer bonding energies (ILBEs) between DFT-D2 and Giese methods for various sheet structure minerals.

A comparison of ILBE and friction coefficients for layered minerals is plotted in Figure 5. The horizontal axes represent ILBEs calculated by *Giese* [1974, 1978] and DFT-D2 methods. A linear relationship was observed between the friction coefficients measured by *Moore and Lockner* [2004] and the ILBEs calculated by using the Giese method; this relationship was less clear for the friction coefficients measured by *Behnsen and Faulkner* [2012]. A linear relationship could not be observed

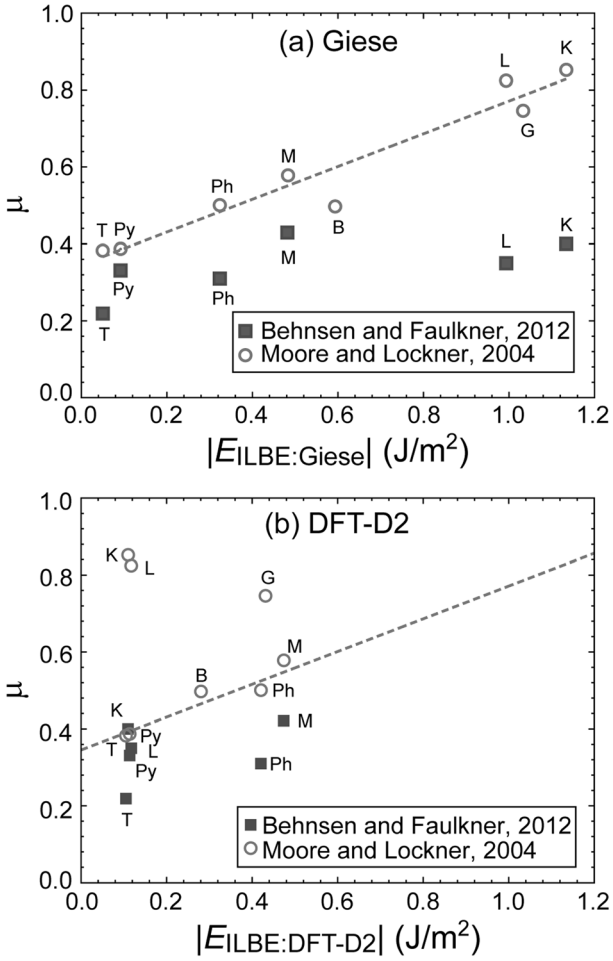

Figure 5. Comparison of experimental friction coefficients and calculated interlayer bonding energies (ILBEs) determined by using methods of (a) *Giese* [1974, 1978] and (b) DFT-D2. The broken line indicates the linear relationship between ILBEs calculated by Giese ($E_{ILBE:Giese}$) and the frictional coefficient measured by *Moore and Lockner* [2004]. In these figures, labels (Py: Pyrophyllite; T: Talc; K: Kaolinite; L: Lizardite; G: Gibbsite; B: Brucite; M: Muscovite; Ph: Phlogopite) near points indicate which point belongs to which particular mineral.

when the friction coefficients were plotted with the ILBE calculated by the DFT-D2 method, as shown in Figure 5b. Therefore, we concluded that the relationship between the ILBEs of layered minerals and experimentally measured friction coefficients remains unclear.

4. Implications for the Relationship Between Frictional Coefficients and ILBE

In this paper, we reported reliable ILBE for layered-structure minerals. The results indicate no linear relationship between the ILBE and experimentally measured friction coefficients. However, the results do not remove the possibility of the relationship between ILBE and friction coefficients because the friction coefficient used for comparing the ILBE was obtained by experiments conducted under various conditions. A simulation conducted by *Abe and Mair* [2009] based on the lattice solid model indicated that the friction parameters acting between spherical particles are insensitive to macroscopic friction. They concluded that gouge grain geometry is a much more important factor than particle-scale friction in establishing the macroscopic friction level. Such a gouge grain is composed by aggregates of spherical particles; thus, the gouge grain geometry would be affected by the strength of the ILBE of the composite minerals.

As previously discussed in friction measurements [*Behnsen and Faulkner*, 2012], mineral shape and size distribution may be related to the results of friction coefficients. Shear experiments for granular gouge layers conducted by *Anthony and Marone* [2005] revealed that quartz particle angularity increased the frictional strength more than that when spherical glass beads were used at low normal stress conditions (<10 MPa). They interpreted that smooth, spherical particles can rotate to accommodate strain, whereas angular grains require dilation for rolling, which increases the bulk frictional resistance [*Anthony and Marone*, 2005]. However, this interpretation is not straightforward in layered minerals, particularly at high effective normal stress conditions (>20 MPa). Low-friction coefficients of 0.3–0.6 at low normal stress (10 MPa) were observed for layered minerals [*Behnsen and Faulkner*, 2012]. Although the layered minerals show platy morphology rather than the spherical and smooth characteristics of quartz, the frictional strength is lower than the 0.6 value of the quartz particles [*Anthony and Marone*, 2005]. This result appears to be in opposition to the high friction of angular grains observed for quartz gouge.

The behavior of clay minerals under low normal stress may be strongly affected by cohesion of the minerals. The cohesive strength of clay minerals depends on applied stress during consolidation and affects the frictional strength under applied normal stress [*Ikari and Kopf*, 2011]. Therefore, it is difficult to apply the friction mechanism of quartz particles to layered minerals at low normal stress.

The degree of rotation, which is a key factor deduced by the shear measurement of quartz gouge, should be important for the friction coefficient of clay minerals under high normal stress. An increased friction coefficient of pyrophyllite gouge was observed, which may be attributed to the presence of (001) planes perpendicular to the shear surface under high normal stress (100 MPa) [*Moore and Lockner*, 2004]. This result indicates that the low frictional strength of layered minerals can be explained by low friction between the basal planes and a high degree of preferred orientation, which may be related to the particle size and geometry relative to the ILBE. We consider that the carefully controlled size and shape distribution of minerals should be used for friction measurements to reveal the relationship between the friction coefficient and ILBE.

5. Conclusions

In this study, the ILBEs of layered minerals were precisely calculated by using the DFT method. To derive the ILBEs of talc and pyrophyllite, van der Waals force is critical to the DFT method. The ILBEs calculated by using the Giese method for hydrogen-bonding minerals such as kaolinite, lizardite, gibbsite, and brucite strongly overestimated the reliable energies calculated by the DFT method. This result should be ascribed to the inaccurate approximation of the point charges at the basal planes. A linear relationship between experimentally measured friction coefficients of layered minerals and the ILBEs determined by using the Giese method was not confirmed in this study. This result does not remove the possibility of the relationship between ILBE and friction coefficients, however, because the friction coefficient used for comparing the ILBE was obtained by experiments conducted under various conditions. The ILBE derived from the DFT method should be used in future studies for discussing the relationship between the energy and frictional strengths of layered minerals.

Acknowledgments

All calculations were performed by using the code Quantum Espresso [*Giannozzi et al*., 2009] and VASP [*Kresse and Hafner*, 1993; *Kresse and Furthmüller*, 1996]. Data supporting Figures 2–5 are available as Tables S1–S3 in the supporting information. This research was partially supported by the Japan Society for the Promotion of Science (JSPS) Grants-in-Aid for Scientific Research (KAKENHI) 23740390 and 26610172. We thank K. Kawai and I. Katayama for their valuable discussion. Computer resources were provided by TSUBAME2.0 at Tokyo Institute of Technology and by the clusters at the National Institute of Materials Science.

References

Abe, S., and K. Mair (2009), Effects of gouge fragment shape on fault friction: New 3D modelling results, *Geophys. Res. Lett.*, *36*, L23302, doi:10.1029/2009GL040684.

Anthony, J. L., and C. Marone (2005), Influence of particle characteristics on granular friction, *J. Geophys. Res.*, *110*, B08409, doi:10.1029/2004JB003399.

Barone, V., M. Casarin, D. Forrer, M. Pavone, M. Sambi, and A. Vittadini (2009), Role and effective treatment of dispersive forces in materials: Polyethylene and graphite crystals as test cases, *J. Comput. Chem.*, *30*(6), 934–939.

Behnsen, J., and D. R. Faulkner (2012), The effect of mineralogy and effective normal stress on frictional strength of sheet silicates, *J. Struct. Geol.*, *42*, 49–61.

Behnsen, J., and D. R. Faulkner (2013), Permeability and frictional strength of cation-exchanged montmorillonite, *J. Geophys. Res. Solid Earth*, *118*, 2788–2798, doi:10.1002/jgrb.50226.

Bengtsson, L. (1999), Dipole correction for surface supercell calculations, *Phys. Rev. B*, *59*(19), 12,301–12,304.

Bish, D. L. (1993), Rietveld refinement of the kaolinite structure at 1.5 K, *Clays Clay Miner.*, *41*(6), 738–744.

Björkman, T., A. Gulans, A. V. Krasheninnikov, and R. M. Nieminen (2012), Are we van der Waals ready?, *J. Phys. Condens. Matter*, *24*, 424218.

Boutareaud, S., T. Hirose, M. Andréani, M. Pec, D.-G. Calugaru, A.-M. Boullier, and M.-L. Doan (2012), On the role of phyllosilicates on fault lubrication: Insight from micro-and nanostructural investigations on talc friction experiments, *J. Geophys. Res.*, *117*, B08408, doi:10.1029/2011JB009006.

Byerlee, J. (1978), Friction of rocks, *Pure Appl. Geophys.*, *116*, 615–626.

Carpenter, B. M., C. Marone, and D. M. Saffer (2011), Weakness of the San Andreas Fault revealed by samples from the active fault zone, *Nat. Geosci.*, *4*(4), 251–254.

Christenson, H. K. (1993), Adhesion and surface energy of mica in air and water, *J. Phys. Chem.*, *97*, 12,034–12,041.

Dion, M., H. Rydberg, E. Schröder, D. C. Langreth, and B. I. Lundqvist (2004), Van der Waals density functional for general geometries, *Phys. Rev. Lett.*, *92*, 246401.

Frye, K. M., and C. Marone (2002), Effect of humidity on granular friction at room temperature, *J. Geophys. Res.*, *107*(B11), 2309, doi:10.1029/2001JB000654.

Giannozzi, P., et al. (2009), Quantum Espresso: A modular and open-source software project for quantum simulations of materials, *J. Phys. Condens. Matter*, *21*(39), 395502, doi:10.1088/0953-8984/21/39/395502.

Giese, J. R. F. (1974), Surface energy calculations for muscovite, *Nature*, *248*, 580–581.

Giese, R. F. (1978), The electrostatic interlayer forces of layer structure minerals, *Clays Clay Miner.*, *26*(1), 51–57.

Gregorkiewitz, M., B. Lebech, M. Mellini, and C. Viti (1996), Hydrogen positions and thermal expansion in lizardite-1*T* from Elba: A low-temperature study using Rietveld refinement of neutron diffraction data, *Am. Mineral.*, *81*, 1111–1116.

Grimme, S. (2006), Semiempirical GGA-type density functional constructed with a long-range dispersion correction, *J. Comput. Chem.*, *27*(15), 1787–1799.

Grimme, S., J. Antony, S. Ehrlich, and H. Krieg (2010), A consistent and accurate *ab initio* parametrization of density functional dispersion correction (DFT-D) for the 94 elements H-Pu, *J. Chem. Phys.*, *132*, 154104.

Henderson, I. H. C., G. V. Ganerød, and A. Braathen (2010), The relationship between particle characteristics and frictional strength in basal fault breccias: Implications for fault-rock evolution and rockslide susceptibility, *Tectonophysics*, *486*, 132–149.

Ikari, M. J., and A. J. Kopf (2011), Cohesive strength of clay-rich sediment, *Geophys. Res. Lett.*, *38*, L16309, doi:10.1029/2011GL047918.

Ikari, M. J., D. M. Saffer, and C. Marone (2009), Frictional and hydrologic properties of clay-rich fault gouge, *J. Geophys. Res.*, *114*, B05409, doi:10.1029/2008JB006089.

Johnson, E. R., I. D. Mackie, and G. A. DiLabio (2009), Dispersion interactions in density-functional theory, *J. Phys. Org. Chem.*, *22*, 1127–1135.

Klimeš, J., D. R. Bowler, and A. Michaelides (2011), Van der Waals density functionals applied to solids, *Phys. Rev. B*, *83*, 195,131.

Koch, W., and M. C. Holthausen (2001), *A Chemist's Guide to Density Functional Theory*, 2nd ed., Wiley-VCH, Weinheim, Germany.
Kresse, G., and J. Furthmüller (1996), Efficiency of ab-initio total energy calculations for metals and semiconductors using a plane-wave basis set, *Comput. Mater. Sci.*, *6*, 15–50.
Kresse, G., and J. Hafner (1993), Ab initio molecular dynamics for liquid metals, *Phys. Rev. B*, *47*, 558–561.
Kresse, G., and D. Joubert (1999), From ultrasoft pseudopotentials to the projector augmented-wave method, *Phys. Rev. B*, *59*, 1758–1775.
Kummel, S., and L. Kronik (2008), Orbital-dependent density functionals: Theory and applications, *Rev. Mod. Phys.*, *80*(1), 3–60.
Langreth, D. C., M. Dion, H. Rydberg, E. Schroder, P. Hyldgaard, and B. I. Lundqvist (2005), Van der Waals density functional theory with applications, *Int. J. Quantum Chem.*, *101*(5), 599–610.
Lee, J. H., and S. Guggenheim (1981), Single crystal X-ray refinement of pyrophyllite-1*Tc*, *Am. Mineral.*, *66*, 350–357.
Lockner, D. A., C. Morrow, D. Moore, and S. Hickman (2011), Low strength of deep San Andreas fault gouge from Safod core, *Nature*, *472*(7341), 82–85.
Logan, J. M., and K. A. Rauenzahn (1987), Frictional dependence of gouge mixtures of quartz and montmorillonite on velocity, composition and fabric, *Tectonophysics*, *144*(1–3), 87–108.
Louie, S. G., S. Froyen, and M. L. Cohen (1982), Nonlinear ionic pseudopotentials in spin-density-functional calculations, *Phys. Rev. B*, *26*(4), 1738–1742.
Mair, K., K. M. Frye, and C. Marone (2002), Influence of grain characteristics on the friction of granular shear zones, *J. Geophys. Res.*, *107*(B10), 2219, doi:10.1029/2001JB000516.
Milman, V., B. Winkler, J. A. White, C. J. Pickard, M. C. Payne, E. V. Akhmatskaya, and R. H. Nobes (2000), Electronic structure, properties, and phase stability of inorganic crystals: A pseudopotential plane-wave study, *Int. J. Quantum Chem.*, *77*, 895–910.
Monkhorst, H. J., and J. D. Pack (1976), Special points for Brillouin-zone integrations, *Phys. Rev. B*, *13*(12), 5188–5192.
Moore, D. E., and D. A. Lockner (2004), Crystallographic controls on the frictional behavior of dry and water-saturated sheet structure minerals, *J. Geophys. Res.*, *109*, B03401, doi:10.1029/2003JB002582.
Moore, D. E., and D. A. Lockner (2007), Friction of the smectite clay montmorillonite: A review and interpretation of data, in *The Seismogenic Zone of Subduction Thrust Faults*, edited by T. H. Dixon and J. C. Moore, pp. 317–345, Columbia Univ. Press, New York.
Morgan, J. K. (1999), Numerical simulations of granular shear zones using the distinct element method. 2. Effects of particle size distribution and interparticle friction on mechanical behavior, *J. Geophys. Res.*, *104*(B2), 2721–2732, doi:10.1029/1998JB900055.
Morrow, C. A., D. E. Moore, and D. A. Lockner (2000), The effect of mineral bond strength and adsorbed water on fault gouge frictional strength, *Geophys. Res. Lett.*, *27*(6), 815–818, doi:10.1029/1999GL008401.
Odelius, M., M. Bernasconi, and M. Parrinello (1997), Two dimensional ice adsorbed on mica surface, *Phys. Rev. Lett.*, *78*, 2855–2858.
Oohashi, K., T. Hirose, and T. Shimamoto (2013), Graphite as a lubricating agent in fault zones: An insight from low- to high-velocity friction experiments on a mixed graphite-quartz gouge, *J. Geophys. Res. Solid Earth*, *118*, 2067–2084, doi:10.1002/jgrb.50175.
Perdew, J. P., K. Burke, and M. Ernzerhof (1996), Generalized gradient approximation made simple, *Phys. Rev. Lett.*, *77*(18), 3865–3868.
Perdikatsis, B., and H. Burzlaff (1981), Strukurverfeinerung am talk $Mg_3[(OH)_2Si_4O_{10}]$, *Z. Kristallogr.*, *156*, 177–186.
Rappe, A. M., K. M. Rabe, E. Kaxiras, and J. D. Joannopoulos (1990), Optimized pseudopotentials, *Phys. Rev. B*, *41*(2), 1227–1230.
Redhammer, G. J., and G. Roth (2002), Single-crystal structure refinements and crystal chemistry of synthetic trioctahedral micas $KM_3(Al^{3+},Si^{4+})_4O_{10}(OH)_2$, where M = Ni^{2+}, Mg^{2+}, Co^{2+}, Fe^{2+}, or Al^{3+}, *Am. Mineral.*, *87*(10), 1464–1476.
Richardson, S. M., and J. W. Richardson Jr. (1982), Crystal structure of a pink muscovite from Archer's post, Kenya: Implications for reverse pleochroism in dioctahedral micas, *Am. Mineral.*, *67*, 69–75.
Saalfeld, H., and M. Wedde (1974), Refinement of the crystal structure of gibbsite, $Al(OH)_3$, *Z. Kristallogr.*, *139*, 129–135.
Sakuma, H. (2013), Adhesion energy between mica surfaces: Implications for the frictional coefficient under dry and wet conditions, *J. Geophys. Res. Solid Earth*, *118*, 6066–6075, doi:10.1002/2013JB010550.
Shimamoto, T., and J. M. Logan (1981), Effects of simulated clay gouges on the sliding behavior of Tennessee sandstone, *Tectonophysics*, *75*(3–4), 243–255.
Troullier, N., and J. L. Martins (1991), Efficient pseudopotentials for plane-wave calculations, *Phys. Rev. B*, *43*(3), 1993–2006.
Tunega, D., T. Bučko, and A. Zaoui (2012), Assessment of ten DFT methods in predicting structures of sheet silicates: Importance of dispersion corrections, *J. Chem. Phys.*, *137*, 114105.
Vanderbilt, D. (1990), Soft self-consistent pseudopotentials in a generalized eigenvalue formalism, *Phys. Rev. B*, *41*(11), 7892–7895.
Wintsch, R. P., R. Christoffersen, and A. K. Kronenberg (1995), Fluid-rock reaction weakening of fault zones, *J. Geophys. Res.*, *100*(B7), 13,021–13,032, doi:10.1029/94JB02622.
Zigan, F., and R. Rothbauer (1967), Neutronenbeugungsmessungen am brucit, *Neues Jahrb. Mineral. Monatsh.*, *4/5*, 137–143.